
FACULTY OF INFORMATION TECHNOLOGY AND ELECTRICAL ENGINEERING

DEGREE PROGRAMME IN ELECTRONICS AND COMMUNICATIONS ENGINEERING

# MASTER'S THESIS

# DEVELOPMENT OF PRINTING METHODS AND SUBSTRATE TREATMENTS FOR EFFICIENT LI-ION BATTERY SYSTEMS

| | |
|---|---|
| Author | Harri Taponen |
| Supervisor | Rafal Sliz |
| Second Examiner | Pauliina Vilmi |

October 2022

**Taponen H. (2022) Development of Printing Methods and Substrate Treatments for Efficient Li-ion Battery Systems.** University of Oulu, Faculty of Information Technology and Electrical Engineering, Degree Programme in Electronics and Communications Engineering. Master's Thesis, 39 p.

# ABSTRACT

**The manufacturing of Lithium-ion batteries is changing due to environmental concerns. Scientists are seeking non-toxic and environmentally friendly materials to improve the sustainability of battery fabrication. In this thesis, Cyrene was researched as a suitable solvent for the fabrication of cathode layers. Various surface treatments of the substrates were used to increase the wetting of substrates to achieve better printability and, consequently, better cathode layers.**

**After developing and tuning the printing process, the printed cathodes were used to fabricate Pouch batteries. The results indicate that different surface treatments influence the cathode material adhesion to the substrate and overall performance of the batteries.**

**Key words: Lithium-ion, binders, batteries, cathodes, NMC88, solvents, Cyrene, printing.**

**Taponen H. (2022) Painomenetelmien ja substraatin käsittelymenetelmien kehittäminen tehokkaille litiumioniakkujärjestelmille.** Oulun yliopisto, tieto- ja sähkötekniikan tiedekunta, elektroniikan ja tietoliikennetekniikan tutkinto-ohjelma. Diplomityö, 39 s.

# TIIVISTELMÄ

**Litiumioniakkujen valmistamista pyritään muuttamaan ympäristöystävällisemmäksi. Alan tutkijat etsivät myrkyttömiä materiaaleja tehdäkseen akkujen valmistuksesta ympäristön kannalta kestävämpiä. Tässä työssä tutkittiin, soveltuuko Cyrene liuottimeksi katodikerrosten valmistuksessa. Erilaisia pintakäsittelymenetelmiä käytettiin lisäämään substraattien vettymistä paremman painettavuuden ja siten parempien katodikerrosten saavuttamiseksi.**

**Painoprosessin kehitystyön ja säätämisen jälkeen painettuja katodeja käytettiin pussimallin akkujen valmistukseen. Tulokset osoittivat, että erilaiset pintakäsittelyt vaikuttavat katodimateriaalin tarttumiseen substraattiin sekä akkujen yleiseen suorituskykyyn.**

**Avainsanat: Litiumioni, sideaineet, akut, katodit, NMC88, liuottimet, Cyrene, painaminen.**

# TABLE OF CONTENTS

# FOREWORD

This work was done in the Optoelectronic and Measurement Technique Unit of the University of Oulu. The result of the work revealed the possibility of using environmentally friendly materials for the manufacturing of Lithium-ion batteries.

I want to express my best gratitude to my supervisor, Assistant Professor Rafal Sliz, for his guidance and support while pursuing this Master Thesis work. His encouragement helped a lot during this time. I want to express my best gratitude to Doctoral Researcher, Ivy Roy for her guidance and support in practical laboratory work and thesis writing. I want to express gratitude to Professor Tapio Fabritius, Postdoctoral Researcher Pauliina Vilmi, Kari Remes, Esa Hannila and Tero Jakkila for advice and help. I am grateful to the University of Oulu for giving me the possibility to do this Master's thesis.

Oulu, October 12 2022

Harri Taponen

# LIST OF ABBREVIATIONS AND SYMBOLS

| | |
|---|---|
| C | Charging and discharging rate |
| CA | Contact angle |
| $CO_2$ | Carbon dioxide |
| cPVDF | Copolymer poly(vinylidene fluoride) |
| C45 | Carbon-45 |
| DMC | Dimethyl carbonate |
| DMF | Dimethylformamide |
| EC | Ethylene carbonate |
| EMC | Ethyl methyl carbonate |
| FTIR | Fourier Transform Infrared Spectroscopy |
| IoT | Internet of Things |
| IPA | Isopropanol |
| Li-ion | Lithium-ion |
| $LiPF_6$ | Lithium hexafluorophosphate |
| M | Molarity |
| NMC88 | Battery cathode active material composed of Lithium, Nickel, Manganese, Cobalt and Dioxygen |
| NMP | N-Methyl-2-pyrrolidone |
| O | Oxygen |
| PVDF | Polyvinylidene fluoride |
| REACH | Registration, Evaluation and Authorization of Chemicals |
| SEI | Solid electrolyte interphase |
| SEM | Scanning electron microscope |
| UV | Ultraviolet |
| V | Voltage |
| | |
| $c$ | Concentration of solid material in the ink |
| $d$ | Dry film layer thickness |
| $kp$ | Pick-out ratio |
| Sa | Mean roughness |
| Sq | RMS roughness |
| $V_{screen}$ | Theoretical paste volume of a screen |
| $\rho_f$ | Density of the material in a dry film |
| | |
| ° | Degree |
| °C | Degree Celsius |

# 1 INTRODUCTION

## 1.1 Motivation for the work

Energy production and delivery today is changing rapidly. At the same time, the use of electricity in our society is growing, which introduces many problems that need to be solved. One possibility is to resolve problems related to electricity storage and delivery by developing better batteries. The need and market for batteries is continuously growing. Batteries are included in electric systems to provide electricity and ensure the running of our society. Batteries are connected to the electricity grid to offer the possibility to store the electricity. In the near future, cars will be fully electric. These developments are currently ongoing because of global environmental concerns related to Carbon dioxide ($CO_2$) emissions and the batteries are helping to reduce the consumption of fossil fuels. Our society is more connected to the Internet and there is an increasing number of portable devices that need electricity. There are many needs for different batteries and various reasons for developing them. One way to solve some challenges is the introduction of printed batteries.

Printed electronics and batteries are coming into more use for different devices today and will even more so in the future. The printed electronics are basically the printed passive components, capacitors, inductors and resistors. The printed active components include transistors, sensors, and detectors. They are used, for example, to detect humidity, stress, pressure, strain, light, gas concentration and thermal radiation. There are many devices on the market with the need to be lightweight, durable for mechanical stress, and even flexible. [1, 2 p. 39] Some of them, which are implemented in clothes, are possible to remove before washing but often that is not enough, so they have to also be durable during washing cycles.

Printed electronics are involved in energy production, energy harvesting/harnessing like solar cells, wind energy, thermal energy and kinetic energy, and also used in complex level circuits. Another area is functional layers like printed sieves, lenses and photonics. [1, 2 p. 39]

One of the limiting factors of implementing printed electronics is the printing resolution, in cases where sub-micron-size components are needed [3 p. 1].

In the future, the Internet of Things (IoT) needs more suitable solutions for power systems and in most cases, the batteries are involved in the devices. Power systems need to be developed to be durable to mechanical stress, lightweight, environmentally friendly, safe to use, cheap to manufacture, with negligible self-discharge, without memory effects, a long service-life and a higher number of charge/discharge cycles. [1 p. 7, 4 p. 1]

Current printed batteries are mostly based on lithium-ion (Li-ion) architecture: the electrochemistry based on the lithium ions. While discharging, the lithium atoms are ionized in the anode, separating from electrons. The positive ions move via electrolyte through a micro-permeable separator between the cathode and the anode. The ions recombine in the cathode. [5]

The Li-ion batteries have a high energy density and no memory effect like many other batteries. Another advantage includes increased voltage in each cell. Li-ion batteries have large development potential thanks to the number of materials suitable for their electrodes. In addition, Li-ion batteries do not have toxic cadmium and have a very low self-discharge rate. The high energy density is not only an advantage to the Li-ion battery, but also a disadvantage too. A short circuit in the structure can cause an explosion and a danger to users. Aging and cycling cause a loss of capacity in Li-ion batteries. Finally, the manufacturing costs are still relatively high and need to be reduced. [5, 6, 7]

### 1.2 Replacing the use of toxic solvents in the battery manufacture processes

N-Methyl-2-pyrrolidone (NMP) has many advantages in various chemical processes and it is widely used in the chemical industry. In the lithium battery industry, NMP is used as a solvent. NMP is highly toxic and was recently added to the restricted substance list of the Registration, Evaluation and Authorization of Chemicals (REACH). [8, 9]

It is important to find a suitable, environmentally friendly replacement for solvents. In the battery industry, the reduction of the fabrication costs is essential as well.

Water has been researched as an environmentally friendly solvent which reduces costs in the battery industry, especially cathode fabrication. Even if there are good results on ultra-low cathodes, the water-based processing has many challenges related to the degradation of the active materials. Water-based processing has been widely used for graphite anodes but not in the fabrication of the cathodes. [8]

The new bio-based solvent, Cyrene, derived from cellulose and does not contain sulphur or nitrogen. It has been shown that the solvent properties of Cyrene are similar to NMP, and it seems promising to research Cyrene for industrial processing. The results show that the use of Cyrene as the solvent to fabricate a cathode is similar to using NMP from the perspective of cycling and cathode material adhesion.

Dimethylformamide (DMF) is one of the solvents used in the Li-ion battery manufacturing processes even though it is on the restricted substance list of REACH. The use of DMF requires less energy than NMP and is safer to use because of the higher ignition temperature in the battery fabrication processes. The lower energy consumption also reduces greenhouse gas emissions in the battery fabrication processes. Comparing DMF and NMP, DMF has lower surface tension and viscosity. The lower surface tension means better wettability but can cause sedimentation of the battery cathode active material composed of Lithium, Nickel, Manganese, Cobalt and Dioxygen (NMC88). Higher amounts of solid materials are found in a cathode slurry because the solvent has a low viscosity. The gelation of the polymer provides protection against sedimentation and provides an even distribution of materials. Printing methods affect the roughness of the samples. The porosity and the surface roughness of the printed cathode affect the battery's electricity features. Calendering in the battery manufacturing process reduces the roughness of the cathodes but improves the long-range electrical contacts. The analysis of solvability has shown DMF's ability as a solvent. [10]

### 1.3 The battery manufacture processes using an environmentally friendly solvent

Cyrene has been researched as an environmentally friendly solvent to formulate ink. It was used to investigate the possibility of replacing NMP as a solvent. Importantly, the Cyrene is used as a solvent to print the cathode on the aluminium substrate without losing capacity of the Li-ion batteries during charge/discharge cycles. However, the use of Cyrene as the solvent in the ink reduces adhesion and cohesion. The high surface tension of Cyrene can cause problems with wetting. These are critical parameters for good results in battery cell manufacturing. [8] To compensate for the lack of adhesion, surface treatment is introduced.

The use of Cyrene as the solvent causes delamination problems in the printed cathode. In the case of the environmentally friendly solvent, Cyrene has a high boiling point, increasing energy consumption in the battery manufacturing processes. [10, 11 pp. 4054 – 4055]

## 1.4 Researching Cyrene as a solvent

In this thesis, Cyrene was researched to formulate ink and print a cathode on the aluminium foil substrate. Plasma, ultraviolet (UV) and citric acid treatments of the substrates were researched in order to improve adhesion. Consequently, these results were compared with the untreated substrates. Good wetting and adhesion are important factors for a good printing result. The ink must have the appropriate particle size and viscosity for the used printing method. The right ratio of the active material, the conductive material, the solvent and the binder was investigated to formulate optimal ink for screen printing. After printing and conducting characterization, the printed cathodes were used to assemble battery cells. The battery cells were cycled to investigate the loss of capacity.

A One Pouch Cell was the battery appearance after fabrication of the cell (size 44 x 61 $mm^2$). The anode was made of graphite and, as an electrolyte, was made of 1.15 Molarity (M) Lithium hexafluorophosphate ($LIPF_6$) in Ethylene carbonate/Dimethyl carbonate/Ethyl methyl carbonate (EC/DMC/EMC) (ratio 2:4:4) and 1 % Vinylene carbonate. The battery was assembled in a dry room at a temperature of 25 degree Celsius (°C). [10]

The battery cells were charged and discharged using various amounts of constant current until the various cut-off voltages were reached. After a certain number of charged and discharged cycles, the loss of capacity was calculated. Charging and discharging rate (C) is the constant current versus time when the battery in testing is fully charged or discharged [12]. A Maccor Series 4000 battery cycler was used in the cycling process [10].

## 1.5 The structure of this thesis

This thesis has five chapters. Chapter 1 provides an introduction and the structure of this thesis. Chapter 2 contains information about the methods used during experimentation. Ink raw materials were researched as well as the suitable mixing ratio. The behaviour of the raw materials in different temperatures during fabrication was researched as well as its influence on the final ink. In chapter 3, the results of various cathode characterization methods and manufactured batteries are presented.

Chapter 4 includes discussion about the results, the expected results and the differences between them. There is discussion on how to use Cyrene as a solvent for Copolymer poly(vinylidene fluoride) (cPVDF). The effects of the plasma treatment, UV treatment and citric acid treatment on the wetting of the substrates is discussed. This chapter also discusses the results of research into viscosity. The summary compares the used methods and discusses potential improvements. The chapter also compares the materials used and discusses which would be best for final products. Chapter 5 has a summary of the achieved results and concludes.

# 2 METHODS

In this chapter, information regarding the methods used for making the ink, the methods used for the treatments to the substrates, and the utilized printing method is given. In addition, information about the fabrication of the printed samples is provided. Various methods for the characterization of the cathode samples and the substrates are introduced.
Cyrene was researched as a solvent. Copolymer poly(vinylidene fluoride) was used as a polymer because Cyrene did not work as a solvent for Polyvinylidene fluoride (PVDF). NMC88 was used as an active material and Carbon-45 (C45) was used as a conductive material in the ink. Different surface treatment methods for the substrates were researched in this thesis. Plasma and ultraviolet treatment were used for cleaning and increasing the surface energy of the substrates. Citric acid treatment were used to clean the surface of the substrate. Screen printing was used as a printing method. As the characteristic method, a drop shape analyzer was used to research and measure the surface contact angles (CA) on the different treated substrates. An optical microscopy was used to research the surface on the printed samples. The adhesion test was done by utilizing Kapton tape. A scanning electron microscope (SEM), the Fourier Transform Infrared Spectroscopy (FTIR) and a 3D optical profilometer were used to research the untreated and the treated substrates. The cells of batteries were tested by cycling tests.

## 2.1 Ink fabrication

The utilized printing method needs the correct viscosity and appropriate particle sizes of the material in the ink slurry. The ink preparation was started by mixing the solvent and polymer with a magnetic steering bar and temperature-controlled hot plate. The effect of the temperature was researched during mixing. The dry mixed carbon and the active cathode material were poured into the same container with the solvent and the polymer. Then, the ingredients were mixed by using the stirring plate.

To recognize the right viscosity of the slurry, smaller amounts of the different ink composition were initially tested. Different solvent ratios to solid were used to formulate the inks. The other solid materials were used in the same ratio. The mixing time after adding the active and conductive materials affected the viscosity of the slurry.

### *2.1.1 Fabrication of ink for finding the viscosity*

The inks slurries were made with the following ingredients: NMC88 + C45 + cPVDF (ratio 92:4:4). The amount of the ingredients of the first fabricated inks are presented in tables 1, 2, 3, 4, 5, 6, 7 and 8.

In the case of ink 1 and ink 2, Cyrene and cPVDF were mixed at 50 °C for 24 hours. The dry-mixed NMC88 and C45 were mixed into Cyrene and cPVDF at room temperature for 24 hours.

Table 1. The ingredients of fabricated ink 1

| **Cyrene [ml]** | **cPVDF [mg]** | **NMC88 [mg]** | **C45 [mg]** |
|---|---|---|---|
| 2.5 | 133.3 | 3067 | 133.3 |

Table 2. The ingredients of fabricated ink 2

| **Cyrene [ml]** | **cPVDF [mg]** | **NMC88 [mg]** | **C45 [mg]** |
|---|---|---|---|
| 3 | 133.3 | 3067 | 133.3 |

In the case of ink 3 and ink 4, Cyrene and cPVDF were mixed at 50 °C for 24 hours. The dry-mixed NMC88 and C45 were consequently mixed with Cyrene and cPVDF at room temperature for 24 hours.

Table 3. The ingredients of fabricated ink 3

| **Cyrene [ml]** | **cPVDF [mg]** | **NMC88 [mg]** | **C45 [mg]** |
|---|---|---|---|
| 8.4 | 400 | 9200 | 400 |

Table 4. The ingredients of fabricated ink 4

| **Cyrene [ml]** | **cPVDF [mg]** | **NMC88 [mg]** | **C45 [mg]** |
|---|---|---|---|
| 9 | 400 | 9200 | 400 |

In the case of ink 5 and ink 6, Cyrene and cPVDF were mixed at 50 °C for 24 hours. The dry-mixed NMC88 and C45 were mixed with Cyrene and cPVDF at room temperature for 36 hours.

Table 5. The ingredients of fabricated ink 5

| **Cyrene [ml]** | **cPVDF [mg]** | **NMC88 [mg]** | **C45 [mg]** |
|---|---|---|---|
| 4.8 | 268 | 6134 | 268 |

Table 6. The ingredients of fabricated ink 6

| **Cyrene [ml]** | **cPVDF [mg]** | **NMC88 [mg]** | **C45 [mg]** |
|---|---|---|---|
| 5.2 | 268 | 6134 | 268 |

In the case of ink 7 and ink 8, Cyrene and cPVDF were mixed at 50 °C for 24 hours. The dry-mixed NMC88 and C45 were mixed with Cyrene and cPVDF at room temperature for 24 hours.

Table 7. The ingredients of fabricated ink 7

| **Cyrene [ml]** | **cPVDF [mg]** | **NMC88 [mg]** | **C45 [mg]** |
|---|---|---|---|
| 3.8 | 268 | 6134 | 268 |

Table 8. The ingredients of fabricated ink 8

| **Cyrene [ml]** | **cPVDF [mg]** | **NMC88 [mg]** | **C45 [mg]** |
|---|---|---|---|
| 4.2 | 268 | 6134 | 268 |

### *2.1.2 Fabrication of ink with the right viscosity for printing*

For printing trials, the amount of Cyrene was 20 ml, and the other used materials are shown in table 9. The values in the second line are the percentage of the total amount 35.1 g of solid ingredients without Cyrene and the calculated amounts from these by milligrams are in the last row.

Table 9. The ingredients of ink for printing trials

| **NMC88** | **C45** | **cPVDF** |
|---|---|---|
| 92 | 4 | 4 |
| 32292 | 1404 | 1404 |

The final mixing time was 24 hours for Cyrene and cPVDF at 50 °C. NMC88 and C45 were dry mixed for 5 minutes and consequently added to Cyrene and cPVDF for 48 hours of mixing at room temperature. Figure 1 demonstrates the ink consistency.

**Figure 1. The prepared ink consistency.**

## 2.2 Substrate treatments

### *2.2.1 Plasma treatment*

Plasma treatments are used to improve adhesion and wetting properties. In this thesis, a plasma argon method was utilized to prepare the substrate by using a Plasma-Preen II-862 plasma oven. Microwaves generates the plasma and the high-energy argon ions bombard the oxygen atoms in the collision process, reducing the oxides on the surface of the substrate. Plasma treatment removes the organic compounds and the natural oxides that could be further removed by using nitrogen. Plasma treatments increase the surface energy of the substrate prone to absorbing contaminants from the atmosphere into the materials. Aging reduces the effect of the treatment to the surface. [13, 14]

Plasma treatment is a good method for surface modification of the substrate to achieve a good printing result. Plasma treatment is a more effective method than UV-treatment. Importantly, delamination may occur when printing with poor adhesion between the metal surface and the ink materials [15 p. 199].

A 6-minute treatment was used for the plasma-treated substrates. After treatment, the substrates were blown with a nitrogen gun.

### *2.2.2 Ultraviolet treatment*

A UVO-CLEANER 42 device was used in this thesis for UV-treatment of the substrates. This UV + Oxygen (O) cleaning method is powerful for different surfaces. The UV+O cleaning interacts with UV light and molecular oxygen in the air, which generates atomic oxygen and ozone. [16]

To get better wetting results, a lower contact angle needs to be achieved on the surface of the substrate. The ink spreads smoothly and there are less pinholes on the sample. UV-treatments increase the surface energy of the substrate [17].

A 5-minute treatment was used for the UV-treated substrates to the printed samples. After treatment, the substrates were blown with a nitrogen gun.

### *2.2.3 Citric acid treatment*

Citric acid is a non-toxic and renewable raw material. Citric acid-treatment cleans the aluminium substrate from oxide and other particles. [18]

The reaction between aluminium oxide and citric acid is complex. Depending on the pH value of the citric acid, the chemical reaction varies. An important role in the dissolution kinetic is the different surface coordination processes. Oxidation on the surface of the aluminium prevents a chemical reaction between aluminium and water. Aluminium oxidation is soluble in citric acid and helps water to reach the aluminium surface. That chemical reaction gives aluminium hydroxide and hydrogen. [19] The chemical reaction between aluminium and citric acid affects an inhibitor for aluminium corrosion [20 p. 160].

In this thesis, citric acid treatment was conducted by keeping the substrates in a beaker that contained 50 g of citric acid and 1 l of water for 10 minutes. After treatment, the substrates were rinsed with water.

## 2.3 Printing method

Screen printing is a printing technique that produces thin material layers on a flat substrate, making it possible to create multi-layer architectures by repeating the printing process. A screen made of metal or nylon threads is used to define the desired pattern by covering undesired areas of the screen with a light-sensitive emulsion. During the printing process, a paste is forced through the pattern openings by a passing squeegee. The screen printing's key phases in the process are depicted in figure 2. [21]

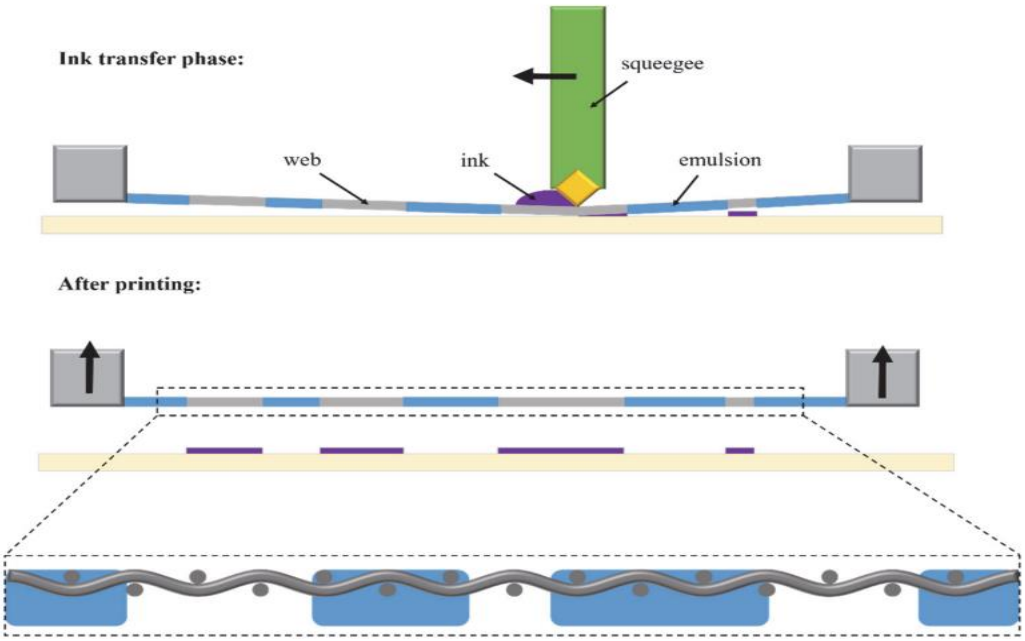


**Figure 2. Screen printing process and a side pattern profile of the printed ink [21].**

The thickness of the final dry film layer $d$ can be estimated from the printed sample film by using equation (1).

$$d = V_{screen} k_p \frac{c}{\rho_f} \tag{1}$$

Where theoretical paste volume of a screen $V_{screen}$ is the volume area of the open screen ($cm^3/m^2$) – the area between the threads of the mesh and the thickness of the wet printed pattern. The pick-out ratio $k_p$ is the amount of material that is set to the $V_{screen}$. The concentration of solid material in the ink is $c$ and the density of material of the final sample film is $\rho_f$. The amount of ink, which $V_{screen}$ considers, affects the speed and force of the squeegee, the snap-off distance between the substrate and the screen, the viscosity of the ink, and the roughness of the substrate. [22 pp. 400 − 401]

In this thesis, Ekra E2 screen printer was used to perform the printing. The settings used are provided in table 10.

Table 10. The used settings of the screen printer

| **Printing speed forward [mm/s]** | **Printing speed backward [mm/s]** | **PCB thickness [mm]** |
|---|---|---|
| 20 | 40 | 0.0 |

In this thesis, the stencil's wires are made of stainless steel. The width of the wire is 50 µm, the mesh width is 80 µm, and there is a 22 µm-thick emulsion layer over the mesh. [23]

The substrates were firstly cleaned by isopropanol (IPA) before printing. The substrates of the samples of UV 4 and Plasma 4 were not cleaned by IPA before printing. The untreated substrates were printed as reference samples. The first printed sample was named as a reference to begin with. The desired thickness of the samples was 70 – 75 µm, excluding the foil thickness. Fifteen samples were printed and after the printing, the samples were dried on a temperature-controlled stirring plate at 100 °C for 60 to 90 minutes.

## 2.4 Characterization methods

The functionality of the printed cathodes was investigated with the various characterization methods provided below. For each method, the operating principles of the devices are briefly introduced.

### *2.4.1 Contact angle measurement*

A drop shape analysis program [24] was used to measure the contact angle to research the wetting on the samples with a KRUSS DSA 100 device. This program calculated the contact angle from the liquid drop on the solid surface and subsequently, the standard deviation was calculated.

The contact angles were measured from the untreated and differently treated substrates using pure Cyrene. Figure 3 shows the contact angle measurement device KRUSS DSA 100.

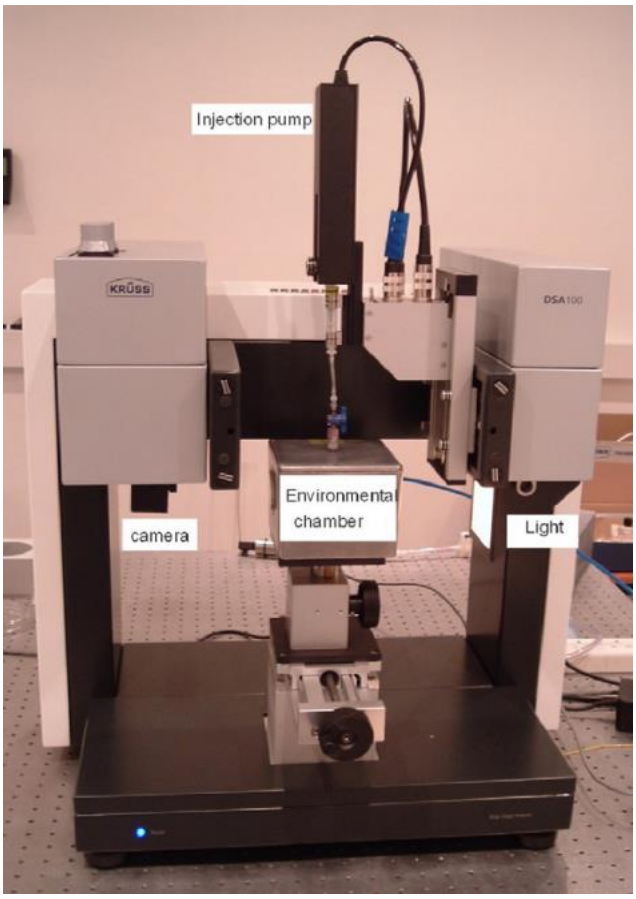


**Figure 3. KRUSS DSA 100 [25].**

### *2.4.2 Optical microscope and profilometer*

A Nikon Eclipse LV100DA-U optical microscope [26] and a ContourGT-K0 3D optical profilometer [27] were used to investigate the visible appearance of the printed samples and their morphology. An optical microscope uses visible light for inspection, which is the reason behind the limited resolution, approximately 200 nanometres, because of the numerical aperture of the conventional lenses. The smaller particles, which need lower resolution, thus require a different method to reconstruct an image [28]. A ContourGT-K0 3D optical profilometer inspects the surface topography with an accuracy between 10 mm and 1 nm [26]. The optical profilometer's 3D pictures were used to research the surface-treated aluminium. The raw 3D-pictures were enhanced with the Gwyddion graphical program. The Nikon Eclipse LV100DA-U optical microscope and ContourGT-K0 3D optical profilometer are presented in figures 4 and 5 respectively.

**Figure 4. Nikon Eclipse LV100DA-U optical microscope [29].**


**Figure 5. ContourGT-K0 3D optical profilometer [27].**

### *2.4.3 Fourier Transform Infrared Spectroscopy*

Fourier Transform Infrared Spectroscopy (FTIR) is a very useful tool for analysing surface composition. Every material has its own molecular level fingerprint. FTIR uses infrared radiation on the surface of the sample and detects a spectrum. The signals of the spectrum are digitalized and analysed by the mathematical technique Fourier Transform. The result is an IR spectrum of intensity versus frequency. The advantages of using this technique are that it is non-destructive, can increase sensitivity, can scan every second, has great optical throughput, gives an accurate measurement, and does not need external calibration. [30] In this thesis, a Thermo Nicolet iS50 FTIR Gold − Spectrometry was used (Figure 6).


**Figure 6. Thermo Nicolet iS50 FTIR Gold Spectrometer [31].**

### *2.4.4 Adhesion test*

An adhesion test was done by using Kapton tape. The peel velocity, the peel angle of the tape, and the ambient temperature were controlled during the test. [32]

In this thesis, the adhesion test was done at the room temperature, the peel velocity was 1 centimetre per second at a 180 degree (°) peel angle.

## 2.5 Surface morphology

A scanning electron microscope is used for the imaging of the material's microstructure and morphology. A low energy electron beam focused on the surface of a sample is scanned by the rays in electrons. [33 pp. 102 − 103]

The SEM detectors capture the scattered signals. The column and the cabinet are the two major parts in the SEM. In the column, the emission occurs and after traversing, the electrons reach the sample. The column is in a vacuum. The detector captures the scanned rays and transfers them as an electrical signal to the cabinet which turns the signals into analysable information in the form of an SEM image. [34 pp. 1 − 7, 35] In this thesis, a JEOLJMC-5000 NeoScope Scanning electron microscope [26] was used (Figure 7).


**Figure 7. JEOLJMC-5000 NeoScope Scanning electron microscope [36].**

## 2.6 Battery manufacture, assembly and testing

The Li-ion battery manufacture and assembly process is composed of three main parts: the electrode manufacturing, the cell assembly and the cell finishing. [37]

In the manufacturing and assembly processes, the highest energy consumption is in the drying and solvent recovery process. The second highest energy consumption is in the drying process where the electrodes are dried to the cell production. These two processes make up approximately three quarters of the total energy consumption of the whole manufacturing and assembly process. The costs of the whole process are more equally divided between the processes than the energy consumptions. The following three processes require the highest expenditure. The highest cost is in the formation and aging process, which consists of charging/discharging, including the solid electrolyte interphase (SEI) process. This is approximately 36.2 % of the total cost. The coating and drying processes in the electrode's manufacturing process are the second most costly, approximately 15 % of the total cost. The enclosing has the third highest cost, approximately 12.5 % of the total costs. The enclosing process is the Li-ion battery packs' assembling process. In the manufacture and assembly of a Li-ion battery, processes need to take into account environmental and recycling aspects. [38]

In this thesis, the ink was fabricated and the substrate treatments were done in a laboratory, in addition to the cathode electrodes being printed and dried. Consequently, the remaining fabrication steps were conducted in the battery laboratory in Kokkola. The final Li-ion batteries were made in a form of Pouch cell in the appendix.

The batteries were tested by cycling tests. The cycling tests start with the formation cycles at a constant current of 0.1 C until a cut-off voltage (4.3 V). Charging continues with constant voltage until the current threshold reaches 0.015 C for the first two cycles. The following cycles were charged with the same methods until the threshold reached 0.02 C. The first discharge cycles were done at the constant current of 0.1 C until 2.6 V was reached. Discharging continued at the constant voltage until the current was below 0.015 C. The battery cells were tested by different rate tests after the formation cycles. After every 100 cycles, the capacity test was done by the cycle of 0.2/0.2 C. By using the theoretical capacities, the C rates were calculated. The tests were done at a temperature of 25 °C. [10]

# 3 RESULTS

This chapter presents the results from various surface characterization methods and the battery cycling test.

## 3.1 Contact angle measurement

Measurements of contact angle tests of Cyrene are shown in table 11. The angles were measured from the surface treated and untreated aluminium foils.

Table 11. The contact angles of pure Cyrene

| **Substrate treatments** | **Average contact angles [°]** | **Standard deviation [°]** | **Comment** |
|---|---|---|---|
| Untreated | 61 | 1.6 | |
| Plasma 6-minute | - | - | CA<5° |
| UV 5-minute | - | - | CA<5° |
| Citric acid | 29.5 | 1.8 | |

In figure 8, there are different substrates for the contact angle measurements: a) the untreated substrate, b) the citric acid-treated substrate, c) the UV-treated substrate, and d) the plasma-treated substrate. The used liquid was Cyrene. The best wetting occurred with the plasma- and the UV-treated substrates, which means a low contact angle. The poorest wetting occurred with the untreated substrate, which means a high contact angle. The values of the contact angles indicate the same results as in table 11.

a)

b)

c)

d)

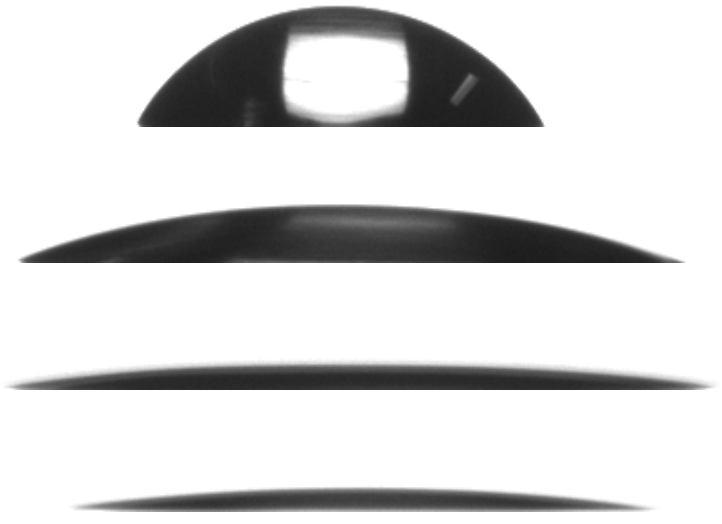

**Figure 8. Contact angle measurements for different treated substrates: a) the untreated substrate, b) the citric acid-treated substrate, c) the UV-treated substrate, and d) the plasma-treated substrate.**

## 3.2 Active cathode material samples

The samples were printed with the ink formulated as described in chapter 2.1.2. The following subchapters discuss the different results achieved during their characterization.

### *3.2.1 Average thickness and standard deviations of the samples*

The thickness of the samples was measured with an electronic micrometric screw. The average thicknesses and standard deviations of the samples were calculated. The values include the thicknesses of the foil which varies between 20 and 25 µm.

The results of the samples on untreated substrates are presented in table 12. Figure 9 shows the "Reference start" sample on untreated substrate. The sample has a smooth printed area without damage to the surface and the edge of the printed area is clear.

Table 12. Reference samples

| **Sample** | **Initial print** | **1** | **2** | **3** |
|---|---|---|---|---|
| Average [µm] | 103.2 | 106.6 | 110.6 | 108.9 |
| Standard deviation [µm] | 3.7 | 2.1 | 2.3 | 2.5 |

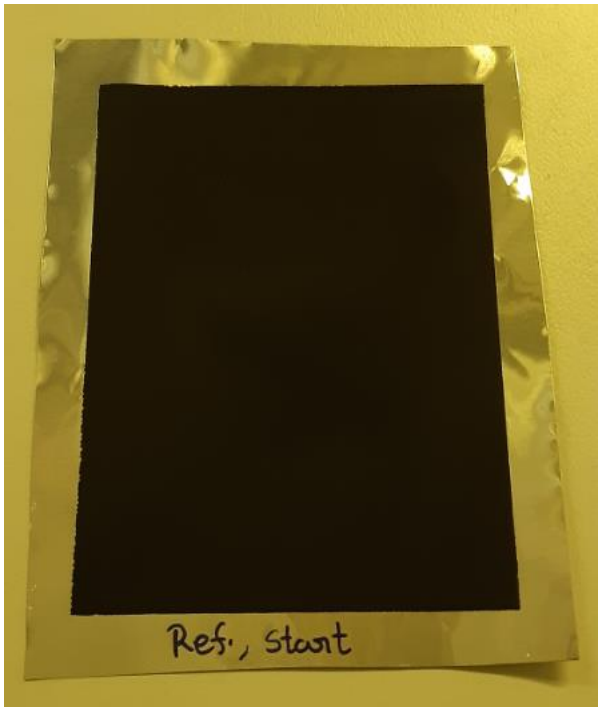


**Figure 9. Reference start, the sample on untreated substrate.**

The results of the samples on plasma-treated substrates are presented in table 13. Figure 10 shows Plasma 2, the sample on plasma-treated substrate. The sample has a smooth printed area, but there are two light instances of damage and a dark line on the surface of the printed area across the sample.

Table 13. Plasma-treated samples

| **Sample** | **1** | **2** | **3** | **4** |
|---|---|---|---|---|
| Average [µm] | 107.7 | 111.2 | 108.9 | 108.7 |
| Standard deviation [µm] | 2.7 | 4.3 | 4.0 | 2.7 |


**Figure 10. Plasma 2, the sample on plasma-treated substrate.**

The results of the samples on UV-treated substrates are presented in table 14. Figure 11 shows UV 3, the sample on UV-treated substrate. The sample has a smooth printed area, but the right side of the printed area is darker than the left side.

Table 14. UV-treated samples

| **Sample** | **1** | **2** | **3** | **4** |
|---|---|---|---|---|
| Average [µm] | 109.7 | 108.3 | 110.3 | 109.6 |
| Standard deviation [µm] | 3.4 | 4.4 | 3.3 | 3.3 |


**Figure 11. UV 3, the sample on UV-treated substrate.**

The results of the samples on citric acid-treated substrates are presented in table 15. Figure 12 shows Acid 3, the sample on citric acid-treated substrate. The sample has a smooth printed area, but there is a lighter area in the middle of the sample.

Table 15. Citric acid-treated samples

| **Sample** | **1** | **2** | **3** |
|---|---|---|---|
| Average [µm] | 106.7 | 102.4 | 102.2 |
| Standard deviation [µm] | 3.1 | 4.9 | 4.7 |


**Figure 12. Acid 3, the citric acid-treated sample.**

### *3.2.2 Optical microscope*

Figure 13 shows a) the smooth area on the sample of the plasma-treated substrate, b) the rough area on the sample of the plasma-treated substrate, c) the smooth area on the sample of the UV-treated substrate, and d) the rough area on the sample of the UV-treated substrate. The printed samples were magnified 100 times with an optical microscope. The images have an uneven distribution of the materials on the samples of the plasma- and the UV-treated substrates.

a) b)

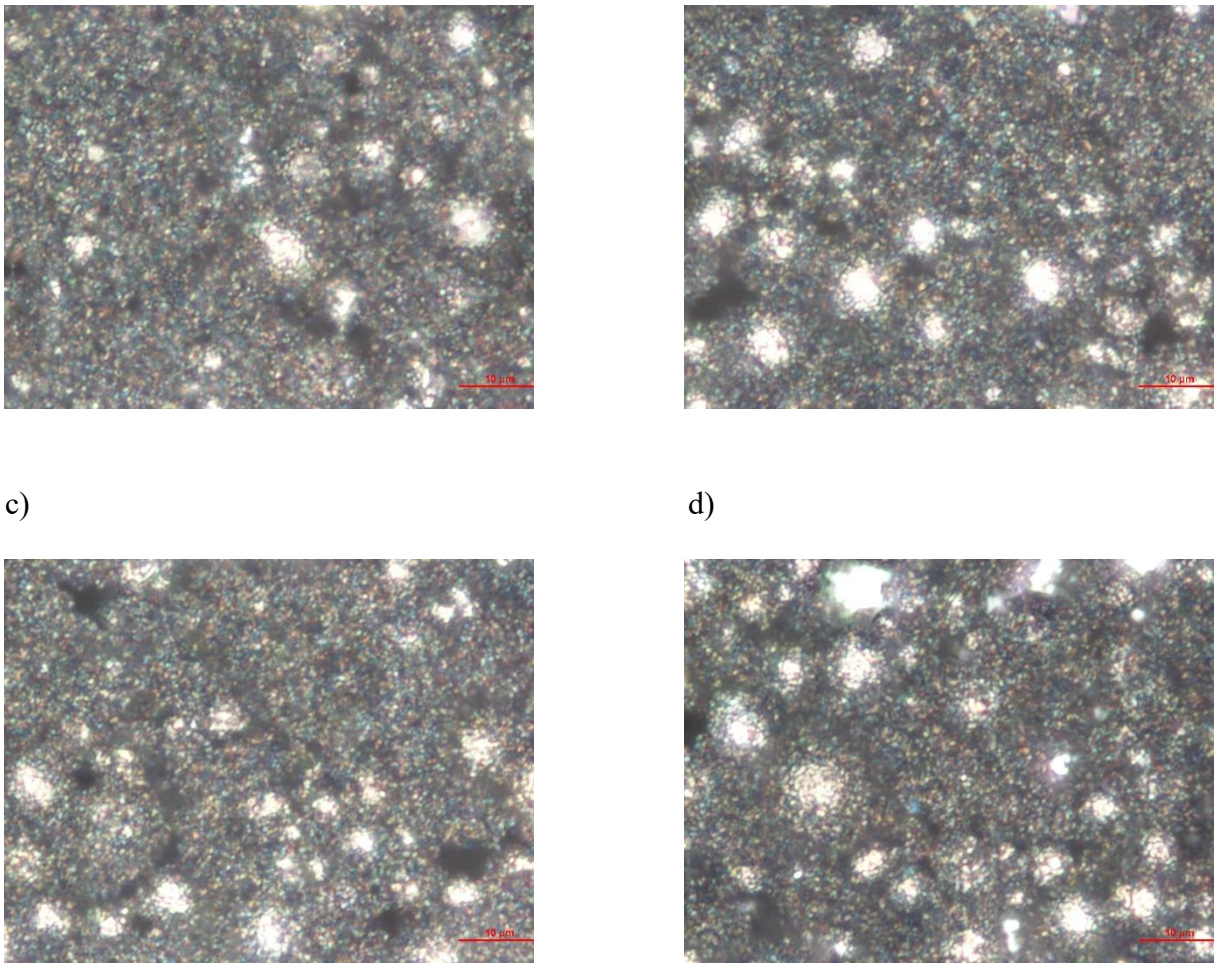

c) d)

**Figure 13. Optical microscope images of the samples on variously treated substrates: a) the smooth area on the sample of the plasma-treated substrate, b) the rough area on the sample of the plasma-treated substrate, c) the smooth area on the sample of the UV-treated substrate, and d) the rough area on the sample of the UV-treated substrate.**

Figure 14 shows a) the smooth area on the sample of the untreated substrate, b) the rough area on the sample of the untreated substrate, c) the smooth area on the sample of the citric acid-treated substrate, and d) the rough area on the sample of the citric acid-treated substrate. The printed samples were magnified 100 times with an optical microscope. The images have less uneven distribution of the materials on the samples compared with Figure 13.

a)

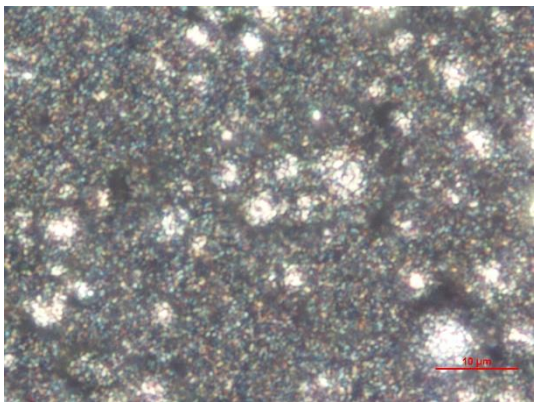

b)

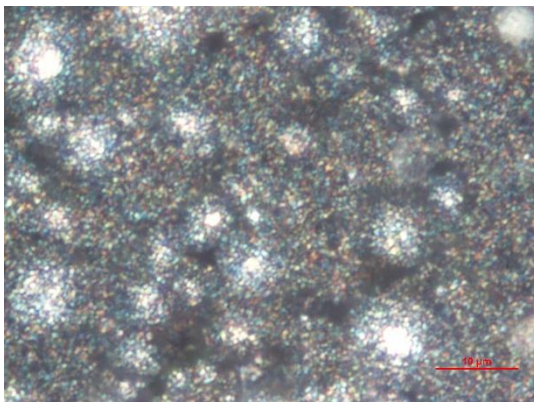

c)

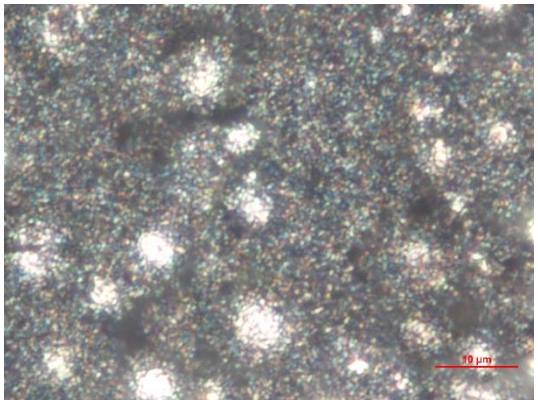

d)

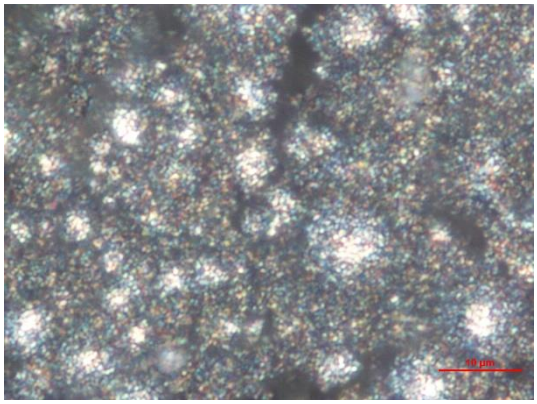

**Figure 14. Optical microscope images of the samples on variously treated substrates: a) the smooth area on the sample of the untreated substrate, b) the rough area on the sample of the untreated substrate, c) the smooth area on the sample of the citric acid-treated substrate, and d) the rough area on the sample of the citric acid-treated substrate.**

### *3.2.3 Adhesion test*

The results of the adhesion test are shown in figure 15. The adhesion test was conducted on four different treated samples. The middle point of the Kapton tape indicates good adhesion in the Reference start sample. For the samples which have the treated substrates, the tests indicate even adhesion on the printed areas.

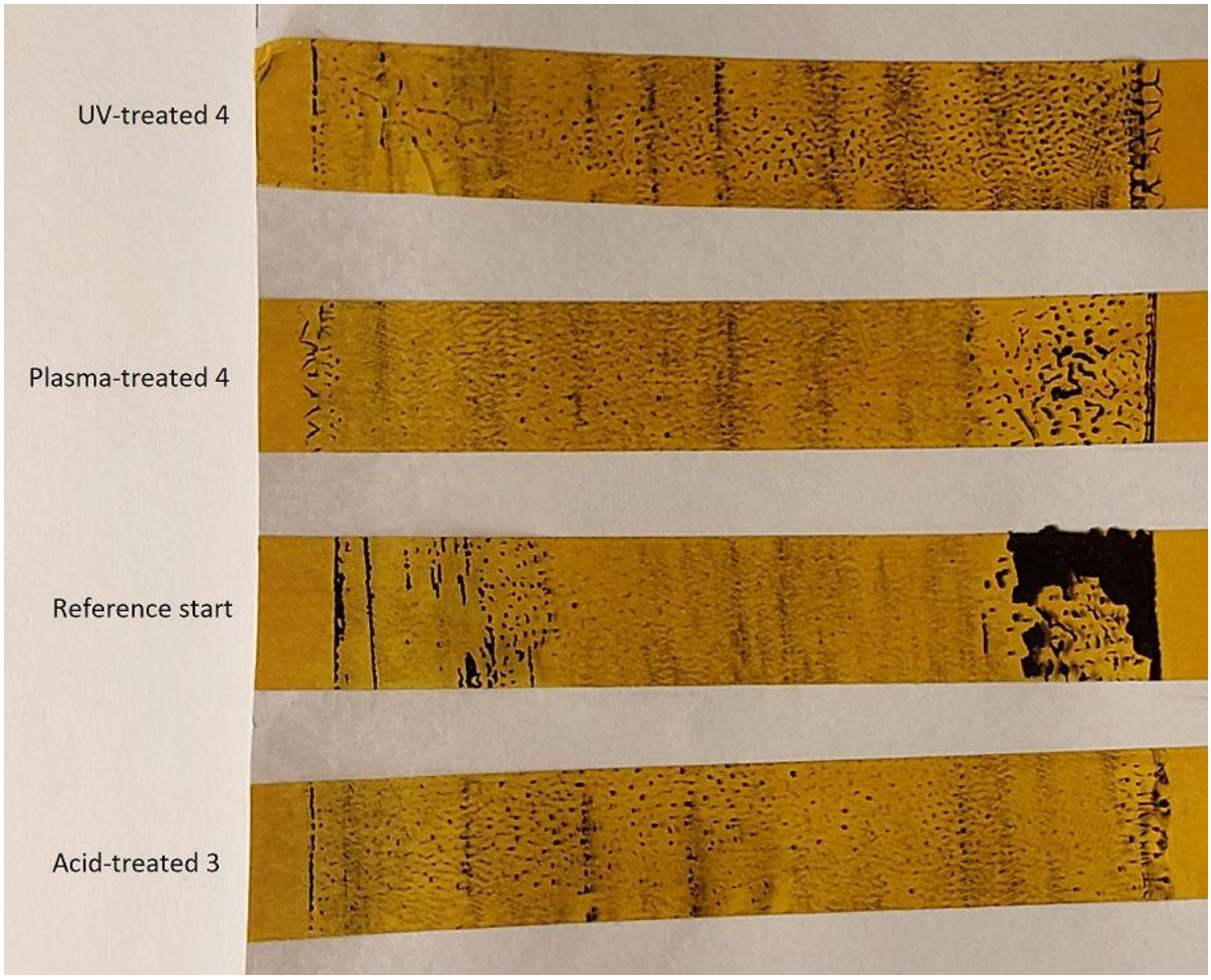


**Figure 15. Adhesion tests on four different samples.**

### *3.2.4 3D optical profilometer*

In figure 16, there are enhanced 3D optical profilometer images: a) the untreated substrate, b) the plasma-treated substrate, c) the UV-treated substrate, and d) the citric acid-treated substrate. The blue colour indicates the lowest points and the red colour the highest points in the scale of the images. Polynomial background was removed by "Maximum polynomial degree of 10" and by "Masking: Use entire image" (ignore mask). Filtering was done by five pixels of the mean value and "Masking mode: Exclude masked region". The colour map shows the many red coloured points on the untreated substrate. On the plasma-treated substrate, the colour map shows more blue coloured areas than the other substrates.

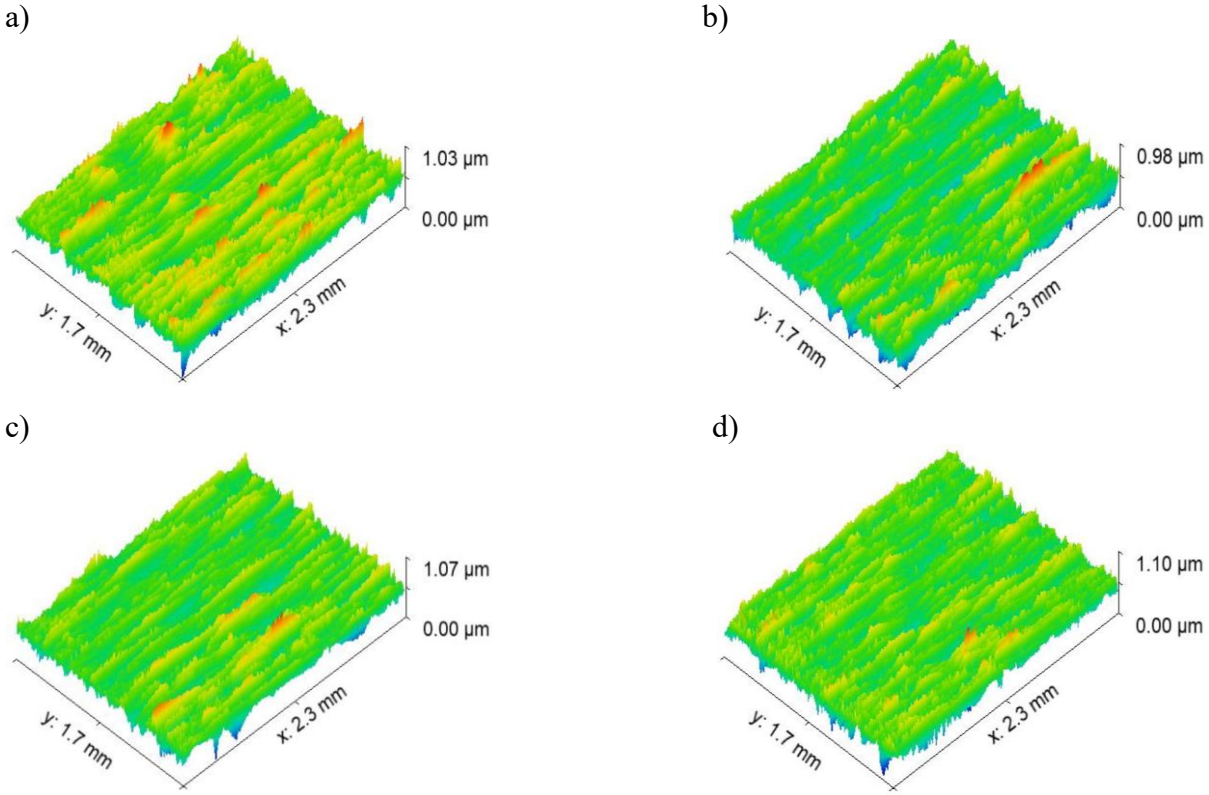


**Figure 16. 3D optical profilometer images of variously treated substrates: a) the untreated substrate, b) the plasma-treated substrate, c) the UV-treated substrate, and d) the citric acid-treated substrate.**

The mean roughness (Sa) and RMS roughness (Sq) of the above figures were calculated in Gwyddion and are presented in table 16.

Table 16. Mean roughness (Sa) and RMS roughness (Sq) values of the above figures

| **Sample** | **Untreated** | **Plasma-treated** | **UV-treated** | **Citric acid-treated** |
|---|---|---|---|---|
| (Sa) [nm] | 83 | 79.6 | 75.7 | 79.7 |
| (Sq) [nm] | 106 | 102.2 | 97.2 | 101.8 |

### *3.2.5 Fourier Transform Infrared Spectroscopy*

The results of FTIR-test for different treated substrates are shown in figure 17. The plasma-treated substrate absorbed more infrared radiation at wavelengths of 1250 – 4000 $cm^{-1}$ than the other substrates. The vibrations of the absorption curves are at the same wavelengths on every substrate.

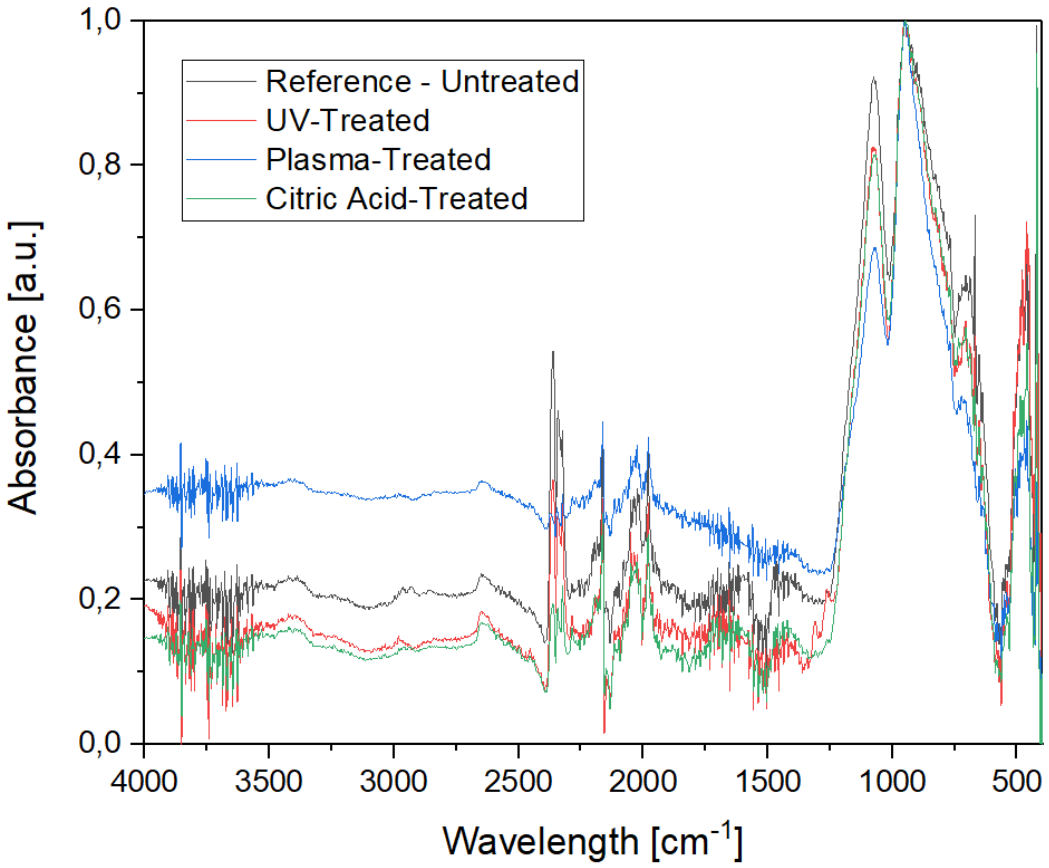


**Figure 17. FTIR-tests for different treated substrates.**

### 3.3 Surface characteristic with SEM

The substrates were magnified 1000 times with an SEM, as shown in figure 18: a) the untreated substrate, b) the plasma-treated substrate, c) the UV-treated substrate, and d) the citric acid-treated substrate. The SEM images show that there are more cracks on the surfaces of the treated substrates than on the surface of the untreated substrate.

a) b)

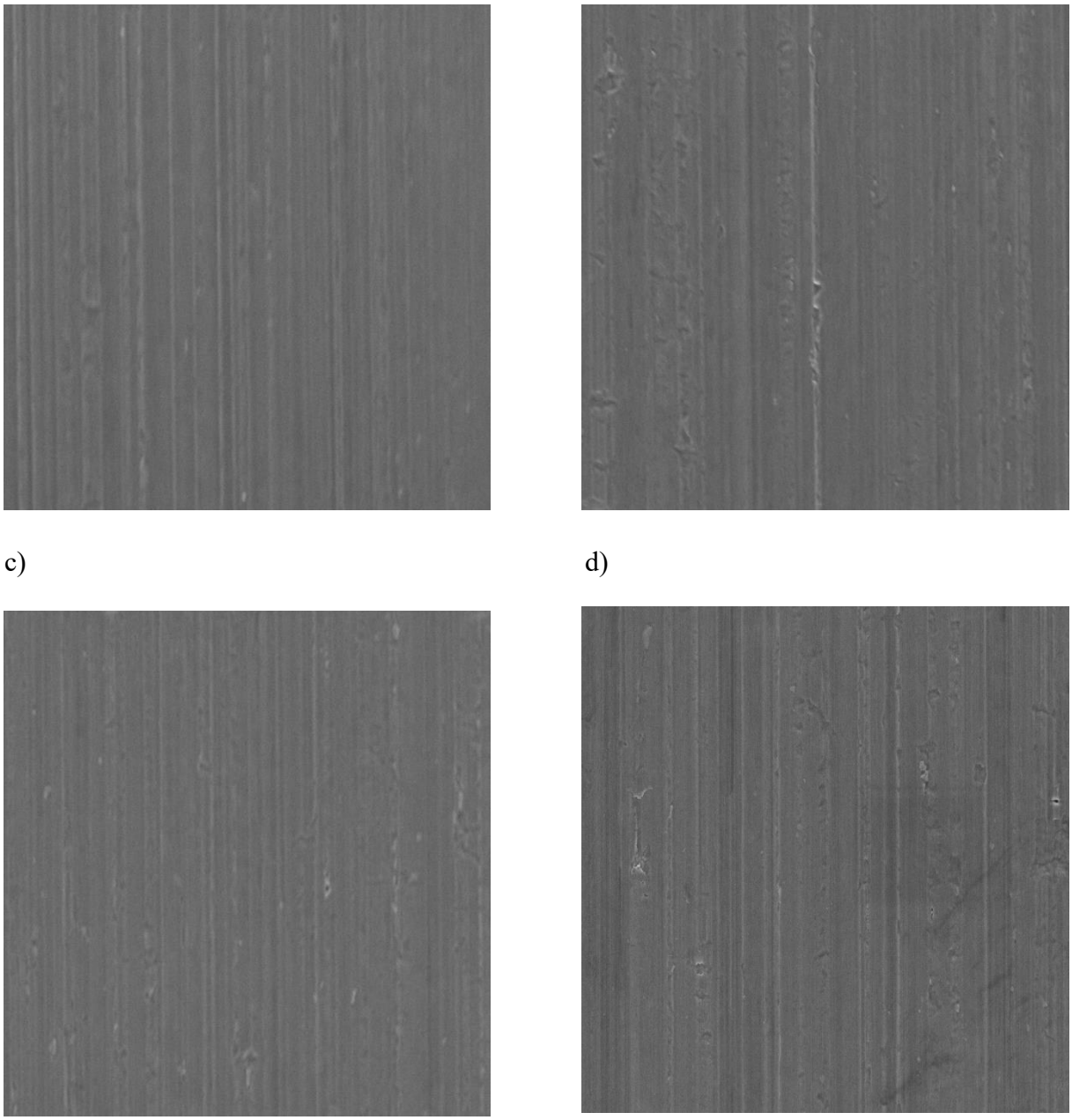

c) d)

**Figure 18. SEM images of variously treated substrates. a) The untreated substrate, b) the plasma-treated substrate, c) the UV-treated substrate, and d) the citric acid-treated substrate.**

### 3.4 Battery cycling tests

Figure 19 shows the capacity results of cycling tests of the different Pouch cells for 300 cycles after the formation cycles. The Pouch cells were made of samples of the different treated substrates. Figure 19 indicates that UV- and plasma treatment affected the capacity of the printed samples.

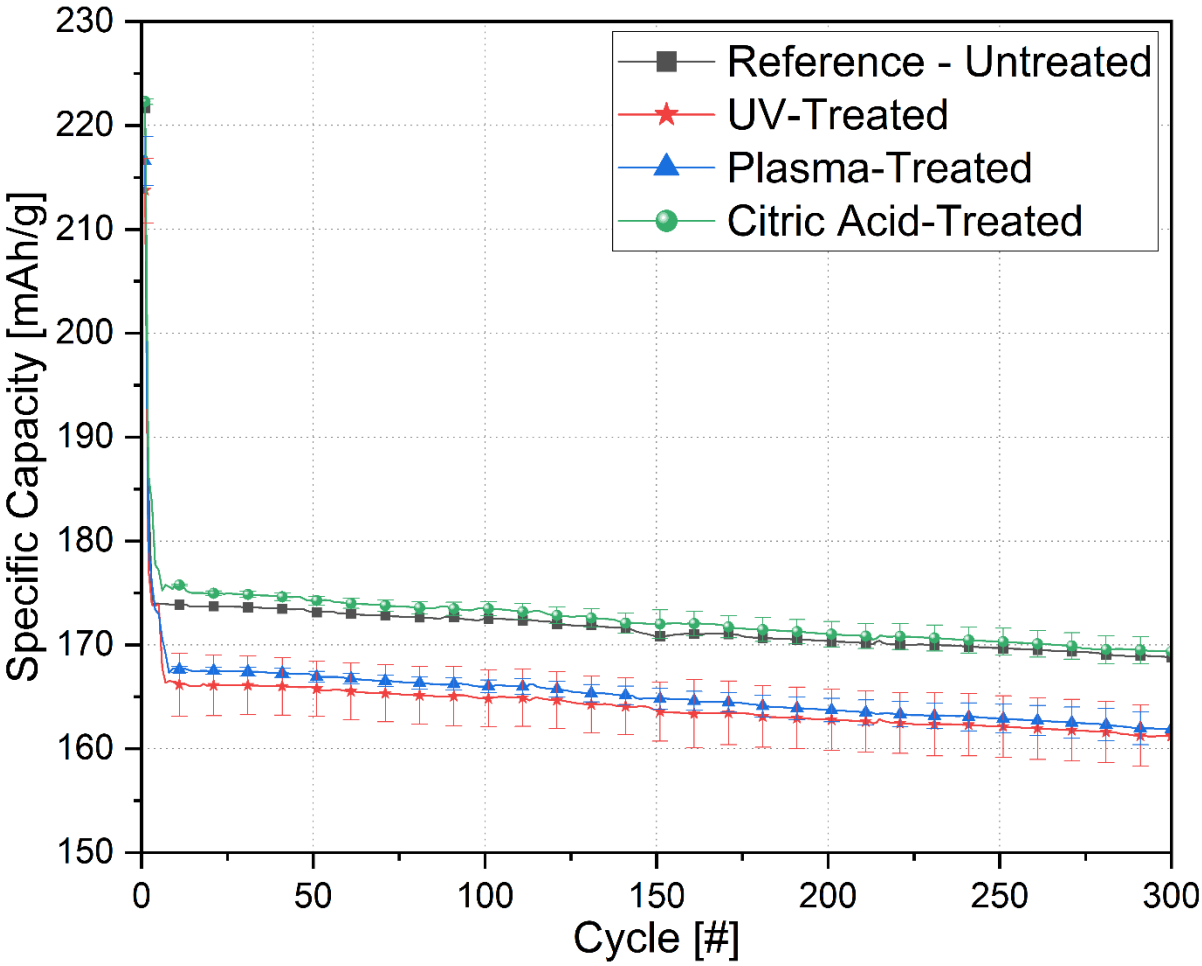


**Figure 19. The capacity results of cycling tests of the different Pouch cells for 300 cycles after the formation cycles.**

# 4 DISCUSSION

While fabricating the ink, it was recognized that the solvent and polymer need a higher temperature than room temperature. The longer mixing time of NMC88 and C45 into the solvent and polymer gave a better viscosity of the ink for further screen printing.

The contact angle measurements indicate that the surface treatments affected the wetting on the substrates. The results of contact angle measurements of the different treated substrates were as expected. The untreated substrate had the poorest wetting comparing to the treated substrates. After printing and drying, the images of the different samples indicate good printing results.

The reason for the light reflection spots in the optical microscope pictures is nickel, one of the compounds of the NMC88 material. The dark reflection spots in the pictures are carbon, which come from C45. The untreated printed samples and the samples of the citric acid-treated substrates had higher surface roughness than the other samples. The surface roughness can be one factor for improving capacity during the cycling tests, while another aspect might be related to the even distribution of the materials on the sample's surface. The uneven distribution of the materials on the sample's surface might be related to problems with the fabrication of the ink. Figure 13 indicates uneven distribution of the materials on the samples, which might explain the smaller capacity of the plasma- and the UV-treated Pouch cells. Figure 11 shows the right side of the printed area is darker than the left side of the sample. It might indicate a drying problem of the sample.

The colour map of the 3D pictures suggest that the plasma treatment removed more material and impurities from the surface of the substrate than other treatments. The numerical values of surface, Sa, are in agreement with the plotted 3D images.

On the image of the FTIR-results, the normalized scale of absorption is on the y-axis and the wavelength is on the x-axis. The wavelengths of 600 – 1500 $cm^{-1}$ are called the fingerprint area. To recognize more specific wavelengths in that fingerprint area, there is strong absorption at the wavelengths of 600 – 800 $cm^{-1}$, 1000 – 1200 $cm^{-1}$ and 1300 – 1600 $cm^{-1}$. These follow the absorption band in the range of 2000 – 2500 $cm^{-1}$, which is the triple bond region. The wavelengths of 1600 – 1650 $cm^{-1}$ have strong intensity, which indicates double bonds or aromatic compounds. Aromatic rings between 1495 $cm^{-1}$ and 1615 $cm^{-1}$ come out of two absorption bands around wavelengths of 1600 – 1500 $cm^{-1}$ and usually follow weak or moderate absorption at wavelengths of 3000 – 3150 $cm^{-1}$. The vibration in the wavelength area of 670 – 850 $cm^{-1}$ with medium to strong intensity of one, or many, absorption bands supports the aromatic absorption band. The absorption bands are strong on the reference substrate at the wavelengths of around 2300 $cm^{-1}$ and 1600 $cm^{-1}$. [39]

It is quite likely that the surface of the aluminium foil has residual rolling oils and oxidation. The FTIR-tests are in agreement with the absorption of oils on the surface of the substrates depending on the substrate treatments. The plasma-treated substrate has less absorption and the strongest absorption was found in the untreated substrate at a wavelength of around 700 $cm^{-1}$. The same conclusion can be made by the absorption at a wavelength of around 1000 $cm^{-1}$. The absorption in the wavelength area of 700 $cm^{-1}$ – 1200 $cm^{-1}$ might indicate oxidation on the surface of the substrate as well. [40, 41, 42, 43]

Generally, the plotted absorptions have the same curve shapes but different absorption levels. In some wavelengths, the substrates have different peaks of absorption.

In the adhesion tests, it is possible to recognize the start and ending of the peel of the tape on every sample. The Reference sample had less adhesion than the other samples, as expected. The adhesion tests did not show many differences between those samples, maybe because the

substrates of Plasma 4 and UV 4 samples were not cleaned by IPA before printing. In further studies, the adhesion test might give different results at a 90° peel angle.

In the surface morphology images, the citric acid treatment did not clean the surface of the foil properly or there has been a problem during the manufacturing process of the aluminium foil. The SEM images show that the surface treatments affected the substrates.

The Pouch cell-cycling test indicates the same shape on the formation cycles except the Pouch cell of the reference sample. The reference Pouch cell reached stable capacity level before the other cells. The reference and the citric acid-treated Pouch cells had very similar capacities. At the same time, the plasma- and the UV-treated Pouch cells showed slightly lower performance. The capacity loss of the different treated Pouch cells was around the same in the tested cycles for 300 cycles. In further studies, it would be important to use a higher number of cycles in order to recognize if the reference and the citric acid-treated cells lose more capacity than the plasma-treated and the UV-treated cells.

# 5 SUMMARY

The utilization of Cyrene in battery fabrication is a promising method that could enable the replacement of toxic solvents currently used, such as NMP or DMF. This research provides evidence that additional treatments of the aluminium substrates result in improved wetting and consequently, better adhesion of the active NMC material. In addition, the conducted electrochemical analysis demonstrates the promising influence of various treatments and the potential of the applied methods. Although further studies are needed, this work demonstrates the potential of printing and the usage of new, sustainable solvents that can revolutionize the battery fabrication process and make them more eco-friendly.

# 6 REFERENCES


[1] Oliveira J. Costa C. M. Laceros-Méndez S. (2018) Printed Batteries: An Overview. In: Laceros-Méndez S. Costa C. Printed Batteries. Materials, Technologies and Applications. John Wiley & Sons Ltd., p. 1 − 20.

[2] Willert A. Tran-Le A. T. Mitra K. Y. Clair M. Costa C. M. Lanceros-Méndez and Baumann R. (2018) Printing Techniques for Batteries. In: Laceros-Méndez S. Costa C. Printed Batteries. Materials, Technologies and Applications. John Wiley & Sons Ltd., p. 21 − 62.

[3] Liu W.C. & Watt A.A.R. (2019) Solvodynamic Printing As A High Resolution Printing Method. SCIENTIFIC REPORTS 9:10766.

[4] Choi K. H. Yoo J. T. Lee C. K. and Lee S. Y. (2016) All-inkjet-printed, solid-state flexible supercapacitors on paper. Energy & Environmental Science 9, 1 – 3.

[5] Clean Energy Institute (read 12.1.2022) What is a lithium-ion battery how does it work? URL: https://www.cei.washington.edu/education/science-of-solar/battery-technology/.

[6] Chen Y. Kang Y. Zhao Y. Wang L. Liu J. Li Y. Liang Z. He X. Li X. Tavajohi N. Li B. (2021) A review of lithium-ion battery safety concerns: The issues, strategies, and testing standards. Journal of Energy Chemistry 59, p. 83 – 99.

[7] Ma S. Jiang M. Tao P. Song C. Wu J. Wang J. Deng T. Shang W. (2018) Temperature effect and thermal impact in lithium-ion batteries: A review. Progress in Natural Science: Material International 28, p. 653 – 666.

[8] Zhou H. Pei B. Fan Q. Xin F. Whittingham M. S. (2021) Can Green Cyrene Replace NMP for Electrode Preparation of NMC 811 Cathodes? Journal of The Electrochemical Society 168 040536.

[9] REACH. Environment (read 18.5.2022) European Commission. URL: https://ec.europa.eu/environment/chemicals/reach/reach_en.htm.

[10] Sliz R. Valikangas J. Santos H. S. Vilmi P. Rieppo L. Hu T. Lassi U. Fabritius T. (2022) Suitable Cathode NMP Replacement for Efficient Sustainable Printed Li-Ion Batteries. ACS Applied Energy Materials, p. 4047 – 4058.

[11] Sliz R. Valikangas J. Santos H. S. Vilmi P. Rieppo L. Hu T. Lassi U. Fabritius T. (2022) Suitable Cathode NMP Replacement for Efficient Sustainable Printed Li-Ion Batteries, Supporting Information. ACS Applied Energy Materials, p. 4047 – 4058.

[12] BU-402: What Is C-rate? (read 8.9.2022) BATTERY UNIVERSITY. URL: https://batteryuniversity.com/article/bu-402-what-is-c-rate.

[13] Ribner A. (read 14.11.2021) Obtaining molecularly clean surfaces by plasma processing. Plasmatic Systems, Inc. URL: https://www.plasmapreen.com/Literature.

[14] Hegemann D. Brunner H. Oehr C. (2003) Plasma treatment of polymers for surface and adhesion improvement. Nuclear Instruments and Methods in Physics Research Section B: Beam Interactions with Materials and Atoms 208, p. 281 – 286.

[15] Bok S. Lim G. H. Lim B. (2017) UV/ozone treatment for adhesion improvement of copper/epoxy interface. Journal of Industrial and Engineering Chemistry 46, p. 199 – 202.

[16] UVO-CLEANER Model 42 SERIES, Instruction manual, Jelight Company, Inc. Irvine, USA.

[17] Heraeus (read 7.8.2022) UV surface pretreatment: cleaning and activation. URL: https://www.heraeus.com/en/hng/light_is_more/how_does_it_work/uv_surface_treatement/pre_treatment_and_activation_of_surfaces.html.

[18] Wikipedia (read 4.8.2022) Citric acid. URL: https://en.wikipedia.org/wiki/Citric_acid#Cleaning_and_chelating_agent.

[19] Petrovic J. Thomas G. (2008) Reaction of Aluminium with Water to Produce Hydrogen. U.S. Department of Energy, Version 1, p. 1 – 26.

[20] Müller B. (2003) Citric acid as corrosion inhibitor for aluminium pigment. Corrosion Science 46 (1), p. 159 – 167.

[21] Vilmi P. (2021) Component fabrication by printing methods for optics and electronics applications. Doctoral Dissertation. University of Oulu, Faculty of Information Technology and Electrical Engineering, Oulu.

[22] Krebs F. C. (2009) Fabrication and processing of polymer solar cells: A review of printing and coating techniques. Solar Energy and Materials & Solar Cells 93, p. 394 – 412.

[23] KOENEN HighTech Screens (read 30.5.2022) Stainless Steel Fabrics. URL: https://www.koenen.de/en/products/meshes-and-frames/stainless-steel-fabrics.html.

[24] KRÜSS (read 26.5.2022) Drop shape analysis. URL: https://www.kruss-scientific.com/en/know-how/glossary/drop-shape-analysis.

[25] David S. Sefiane K. Tadrist L. (2007) Experimental investigation of the effect of thermal properties of the substrate in the wetting and evaporation of sessile drops. Colloids and Surfaces A: Physicochemical and Engineering Aspects 298 (1 − 2), p. 108 – 114.

[26] University of Oulu (read 17.6.2022) Facilities of OPEM. URL: https://www.oulu.fi/en/facilities-opem#MIC.

[27] NON-CONTACT 3D OPTICAL PROFILOMETER (BRUKER, USA). MODEL: CONTOUR GT-K URL: https://teqip-ii.iiests.ac.in/coeteqip/download/lab-equipments/3D-Optical-Profiler-Laboratory.pdf.

[28] Putten E. G. Akbulut D. Bertolotti J. Vos W. L. Lagendijk A. and Mosk A. P. (2011) Scattering Lens Resolves sub-100 nm Structures with Visible Light. American Physical Society. Physical Review Letters 106(19):193905.

[29] MICROSCOPES (read 16.6.2022) NIKON ECLIPSE LV100DA-U. URL: https://www.mccrone.com/product/nikon-eclipse-lv100da-u/.

[30] Dutta A. (2017) Chapter 4-Fourier Transform Infrared Spectroscopy. In: Thomas S. Thomas R. Zachafiah A. Mishra R. Spectroscopic Method for Nanomaterials Characterization. Matthew Deans, p. 73 – 93.

[31] ThermoFisher SCIENTIFIC (read 20.1.2021) Nicolet iS50 FTIR Spectrometer. URL: https://www.thermofisher.com/order/catalog/product/912A0760.

[32] MBK TAPE SOLUTIONS (read 18.2.2021) How to Evaluate and Test Pressure Sensitive Adhesive Tape Performance. URL: https://www.mbktape.com/materials/.

[33] Omidi M. Fatehinya A. Farahani M. Akbari Z. Shahmoradi S. Yazdian F. Tahriri M. Moharamzadeh K. Tayebi L. Vashaee D. (2017) 7-Characterization of biomaterials. In: Tayebi L. Moharamzadeh K. Biomaterials for Oral and Dental Tissue Engineering, p. 97 – 115.

[34] Pereira-da-Silva M. de A. Ferri F. A. (2017) 1-Scanning Electron Microscopy. In: Róz A. L. D. Ferreira M. Leite F. L. Oliveira O. N. Nanocharacterization Techniques, p. 1 – 35.

[35] ThermoFisher SCIENTIFIC (read 15.5.2022) What is SEM? Scanning Electron Microscope Explained. URL: https://www.thermofisher.com/blog/microscopy/what-is-sem-scanning-electron-microscopy-explained/.

[36] NeoScope JCM-5000 (read 30.9.2022) JEOL Serving Advanced Technology. URL: http://www.coherent.com.au/content/media/Nikon/NeoScope%20JCM-5000%20Nikon.pdf.

[37] Heimes H. H. Kampker A. Lienemann C. Locke M. Offermanns C. Michaelis S. Rahimzei E. (read 7.7.2018) Lithium-ion Battery Cell Production Process. URL: https://www.pem.rwth-aachen.de/global/show_document.asp?id=aaaaaaaaabdqbtk.

[38] Liu Y. Zhang R. Wang J and Wang Y. (2021) Current and future lithium-ion battery manufacturing. iScience 24 (4).

[39] Nandiyanto A. B. D. Oktiani R. Ragadhita R. (2019) How to Read and Interpret FTIR Spectroscope of Organic Material. Indonesian Journal of Science & Technology 4 (1), p. 97 – 118.

[40] Enercon (read 12.9.2022) Roll aluminum surface preparation for packaging applications. URL: https://www.enerconind.com/plasma-treating/library/tech-papers-articles/roll-aluminum-surface-preparation-for-packaging.aspx.

[41] Spectro Scientific Ametec (read 13.9.2022) Oil Analysis. URL: https://www.spectrosci.com/fluid-type/oil-analysis-spectro-scientific.

[42] Michael C. G. Bowman J. (2007) FT-IR Analysis of Used Lubricating Oils – General Considerations. Thermo Fisher Scientific, Madison, WI, USA.

[43] INNOVAL (read 14.9.2022) Understanding your aluminium oxide surface. URL: https://www.innovaltec.com/aluminium-oxide-surfaces-blog/.

# 7 APPENDICES

Appendix 1 The Pouch battery cell